Earth-Science Reviews 232 (2022) 104130

Contents lists available at ScienceDirect

Earth-Science Reviews

journal homepage: www.elsevier.com/locate/earscirev

Mantle evolution and continental growth events

Uwe Walzer *, Roland Hendel

Institut für Geowissenschaften, Friedrich-Schiller-Universität, Humboldtstrasse 11, 07743 Jena, Germany

ARTICLE INFO

Keywords:
Continental growth
Episodic
Detrital zircon age
Radial distribution of mantle viscosity
Chemical differentiation
Balance equations

ABSTRACT

This paper presents the computational basis for the study of Walzer and Hendel (2022), who consider the relationships between continental growth, sedimentary geology, natural climate change, and ice ages. Here we solve the full set of balance equations for mass, energy, momentum, and angular momentum for a 3D spherical-shell mantle. The assumed radial distribution of viscosity is given in Appendix B. Furthermore, the modeled viscosity depends on temperature and water concentration. The modeled mantle is internally heated by the radioactive decay of ^{238}U, ^{235}U, ^{232}Th, and ^{40}K. The heat-producing elements are redistributed by chemical differentiation in spatial regions due to partial melting. Thus, in a simplified way, continental material is formed, which accumulates at the surface of a sphere, moves sideways in a non-prescribed way due to flow, and accretes to form continents. The growth curve of the total mass of continental crust resembles that of realistic geological models. We present in Appendix B the Grüneisen parameter, adiabatic temperature, thermal expansivity, and specific heat as a function of depth. The temporal distribution of juvenile additions to the continents, as obtained using our model, has a marked resemblance to global detrital zircon ages published by Puetz and Condie (2019, 2022). The results indicate the continental crust grew in an episodic manner rather than by steady state.

1. Introduction

This paper considers mainly the formation of the continents by chemical differentiation of the mantle. We attempt to show that continent evolution is mainly a consequence of the thermal evolution of the mantle. This process can be numerically modeled by solving the conservation equations of physics. As such, a coherent solution is sought that considers the system as a whole. The energy source for this process begins with the primordial heat of Earth, which originated from the kinetic energy of impacting planetary material and, secondly, the radioactive decay of uranium, thorium, and potassium. The formation of the continents in the middle of the oceans had a profound effect on the evolution of the atmosphere and natural climate change. In turn, climate change drives changes in sedimentary geology. Condie et al. (2021) noted correlations in time-series between detrital zircon ages, orogens, plate velocities, and large igneous provinces (LIPs), and suggested these require a common global process, although the drivers of such cycles remain unclear. In this paper, we numerically explore the relationships between continent generation, detrital zircon ages, and the thermal and chemical evolution of the mantle. This paper provides the theoretical basis for the study of Walzer and Hendel (2022), who examine the relationships between geological processes and natural climate change. Similar to Condie et al. (2021), we show the systematic relationships proposed in previous studies are not consistent with the available data. In this paper, we investigate the generation of juvenile continental crust. For the younger geological record, since ca. 3 Ga, the chemical composition of the continental crust is determined by processes linked to subduction (Rudnick and Gao, 2003) and, to a minor extent, oceanic plateaus. Given that plate motions are relatively uniform, the production of new continental crust should also be relatively constant. However, global detrital zircon crystallization ages show distinct clustering and peaks. Granitoid age peaks defined by thermal ionization mass spectrometry data have even narrower clusters and peaks (Condie et al., 2009). Hawkesworth et al. (2009, 2019) and Cawood et al. (2013) proposed that production of new continental material is approximately constant over time, but that preservation potential is variable. The preservation potential is thought to be greater for late-stage collisional events as supercontinents were amalgamated. In this interpretation, the zircon age maxima do not coincide with peaks of real growth of continental crust, but to time intervals of elevated preservation potential. However, Albarède (1998) argued that oceanic plateaus are entrained with oceanic plates, and these become accreted to the continents during subduction. Silicic magmas are subsequently generated by this process. Therefore, such continental additions appear to be episodic in nature.

* Corresponding author.
E-mail address: u.walzer@uni-jena.de (U. Walzer).

https://doi.org/10.1016/j.earscirev.2022.104130
Received 17 March 2022; Received in revised form 4 July 2022; Accepted 12 July 2022
Available online 16 July 2022
0012-8252/© 2022 Elsevier B.V. All rights reserved.

Arndt and Davaille (2013) suggested that episodic generation of large plumes occurs from a layer above the core–mantle boundary (CMB). These plumes produced komatiites and basalts preserved in greenstone belts. The plumes indirectly caused an acceleration of plate motion and associated subduction, as well as distinct pulses of granitic magmatism. Condie et al. (2017) used the Nd isotopic compositions of silicic igneous rocks to determine the proportion of juvenile input into the continental crust. Condie et al. (2017) concluded that accretionary orogens were more abundant than collisional orogens during periods coinciding with zircon age maxima. Juvenile crust is both generated and preserved during the accretion of orogens. Therefore, Condie et al. (2017) interpreted the zircon age peaks to represent peak periods of continental crustal growth. However, in reality, this problem is more complex, as considered in more detail by Walzer and Hendel (2022). Recently, Reimink et al. (2021) used a sample-based analysis to show that zircon abundance trends over time reflect either intermittent zircon production or an instantaneous preservation bias that has an *immediate* effect on the rock record. The geodynamic problem of the plateness of oceanic lithospheric pieces on a spherical shell has already been solved numerically by Walzer et al. (2004). The presence of two internal low-viscosity layers is conducive for plateness and thin sheet-like downwellings.

2. Four diverse types of models

In this section, we present the details of four different types of models that are of consequence to the present paper and Walzer and Hendel (2022). The geosciences consist of different branches with very different methods. This existing diversity is inescapable, and it is not possible to arrive at robust findings without linking the different branches together. Nevertheless, we must be aware of this diversity when drawing the ultimate conclusions.

Various branches of theoretical physics belong to the *first* type of models used here. This first type is able to predict an incredible amount of measurement data with small error margins. Moreover, it is characteristic of this first type that it is able to predict the results of *different* physical phenomena. Third, it is possible to infer the specific physical model from measured data because the measured data have small error bounds. Therefore, this kind of models could be called double exact models. We give some examples to illustrate this.

Two comprehensive and accurate theories of quantum mechanics have been established by Heisenberg (1926b,a) and Schrödinger (1926a, 1926). An early finding was that quantum mechanics could exactly predict the spectrum of hydrogen. Furthermore, the most important features of the periodic table of elements can be elucidated from the atomic model based on quantum mechanics. Wigner (1959) applied group theory to quantum mechanics, and showed how to derive the structure of atomic spectra for the ground and excited states. Based on this theory and on precise measurements of peaks in the solar spectrum, it was possible to quantify the elemental abundances in the present-day photosphere of the Sun. Apart from highly volatile elements, the distribution of elemental abundances in the photosphere and CI carbonaceous chondrites are similar (Lodders et al., 2009; Asplund et al., 2009). The mass concentration ratios of the chemical elements in CM chondrites relative to CI chondrites decrease as a function of 50% condensation temperature at 10^{-4} bar (Lodders et al., 2009). This observation, combined with similar findings, suggests that CI chondrites have the highest abundances of moderately and highly volatile elements in comparison with all other types of meteorites. This result, in addition to photosphere–CI chondrite similarities, suggests that the CI composition, or a derivative of it, could have been the starting chemical composition of Earth. This is fundamental for our assumptions concerning the chemical composition of Earth's mantle, which is the basis for our computational model.

The *second* type of model is based on first principles (e.g., on a branch of theoretical physics or a compatible combination of two such branches), but there is non-negligible uncertainty with respect to some input parameters. This type of model is referred to as a one-sided exact model. We will present a model of the second type in Section 3.

The *third* type consists of various box models. In the case of climate research, it is impossible to solve the full set of conservation equations. Considering only the atmosphere, it is necessary to solve the conservation equations and the Clausius–Clapeyron equation to compute the dependence of the maximum vapor pressure on the air temperature. Furthermore, it is necessary to include the Stefan–Boltzmann Law to estimate the natural greenhouse effect. To simplify complex systems, this third type of model has been introduced where the system is replaced by boxes. These reservoirs are thought to be mixed homogeneously. The energy or material fluxes between the boxes are assumed to be proportional to the concentration differences. The climate model of Strassmann and Joos (2018) is comparatively simple, being a reduced form of a carbon cycle–climate model. There are many climate models and it is difficult to evaluate these, since many of the models are related (Morgenstern et al., 2017). Jiang et al. (2016) evaluated 77 coupled global climate models (GCMs) used in compiling the 3rd to 5th Assessment Reports of the Intergovernmental Panel on Climate Change (IPCC) and assessed whether these models are able to simulate the average and year-to-year variability of surface air temperatures at 2 m above the ground, precipitation over China, and average East Asian monsoon for the last decades of the 20th century. For the temperatures, the more recent GCMs achieved essential improvements. For the precipitation and monsoon, the more recent model runs showed nearly no improvement compared to the older runs. Zhu et al. (2019) investigated the temporal spectrum of observed global surface temperatures using the database of Zinke et al. (2017). They showed that the hierarchy of climate models can produce increased variance in global mean temperatures at low frequencies. Zhu et al. (2019) also confirmed a scaling break between orbital and annual peaks, occurring at about millennial periodicities. One critical element in these models is the unknown initial conditions of the deep ocean. We note that this type of analysis is unreliable if the system is suddenly disturbed from below (e.g., by the generation of a large igneous province [LIP]) or from above (e.g., from outer space).

The *fourth* type of model is stratigraphic models. These are important in determining, for example, the onset and termination of ice ages. Full details of such models are provided by Walzer and Hendel (2022).

3. Model description

The model employed in this study is a one-sided exact model. We solved the full set of balance equations for the 4567 Ma history of Earth's mantle by varying physically reasonable input parameters. Consequently, numerous runs were necessary. We used a combined numerical strategy for modeling convection by solid-state creep in Earth's mantle, as well as partial melting in some regions of the upper mantle. These processes lead to the segregation and formation of the precursors of continental crustal materials, as well as mixing in the remaining mantle. We solved the differential equations relating to infinite Prandtl number convection, using a three-dimensional finite element spherical-shell method that ensures the conservation of mass, momentum, and energy. The mass balance equation is as follows:

$$\frac{\partial \rho}{\partial t} + \nabla \cdot (\rho \vec{v}) = 0 \tag{1}$$

With an anelastic-liquid approximation this simplifies to

$$\nabla \cdot \vec{v} = -\frac{1}{\rho} \vec{v} \cdot \nabla \rho \tag{2}$$

where ρ is density, t is time, and $\vec{v}$ is velocity.

The conservation of momentum can be written as

$$\rho \left(\frac{\partial \vec{v}}{\partial t} + \vec{v} \cdot \nabla \vec{v} \right) = -\nabla P + \rho \vec{g} + \frac{\partial}{\partial x_k} \tau_{ik} \tag{3}$$

where P is pressure, $\vec{g}$ is acceleration due to gravity, and τ_{ik} is the deviatoric stress tensor.

The energy balance can be expressed as

$$\rho\left[\frac{\partial}{\partial t}+\vec{v}\cdot\nabla\right]u=\nabla\cdot\left(k\nabla T\right)+Q-P\nabla\cdot\vec{v}+\sigma_{ik}\dot{\varepsilon}_{ik}+P\nabla\cdot\vec{v} \tag{4}$$

where u is the specific internal energy, k is thermal conductivity, T is absolute temperature, Q is the heat generation rate per unit volume, σ_{ik} are the stress tensor components, and $\dot{\varepsilon}_{ik}$ are the strain rate tensor components. Using thermodynamics, it is possible to obtain Eq. (5) from Eq. (4) without any approximation:

$$\frac{\partial T}{\partial t}=-\frac{\partial\left(Tv_j\right)}{\partial x_j}-\left(\gamma-1\right)T\frac{\partial v_j}{\partial x_j}+\frac{1}{\rho c_v}\left[\tau_{ik}\frac{\partial v_i}{\partial x_k}+\frac{\partial}{\partial x_j}\left(k\frac{\partial}{\partial x_j}T\right)+Q\right] \tag{5}$$

where x_j are the components of the position vector, v_j are the components of the creeping velocity vector, γ is the thermodynamic Grüneisen parameter, and c_v is the specific heat at a constant volume. Notably, the occurrence of c_v in Eq. (5) is in total accordance with the occurrence of c_p (i.e., specific heat at constant pressure) in the commonly used formula for the energy balance. The deviatoric stress tensor can be expressed as

$$\tau_{ik}=\eta\left(\frac{\partial v_i}{\partial x_k}+\frac{\partial v_k}{\partial x_i}-\frac{2}{3}\frac{\partial v_j}{\partial x_j}\delta_{ik}\right) \tag{6}$$

in Eqs. (3) and (5), where η is viscosity.

Appendix A presents a detailed derivation of Eqs. (1)–(7), which are suitable for undergraduate students of physics or geophysics. These equations follow from the basic principles of physics (i.e., the equations express the conservation of mass, momentum, energy, and angular momentum). The numerical values of the material parameters in the equations are given or derived in Appendix B, and were determined from geophysical measurements or mineralogical experiments.

To solve the equations, we used the Terra code of Baumgardner (1983). This code has been advanced by Bunge and Baumgardner (1995). In the multi-grid procedure, prolongation and restriction are handled in a matrix-dependent manner. In this way, it is possible to accommodate the large variations and steps in the coefficients associated with strong viscosity gradients (Yang, 1997). For the formulation of the chemical differentiation, we modified a tracer module developed by Dave Stegman. Further improvements of the simulation of lithospheric plates on a spherical-shell mantle after ca. 3.0 Ga were achieved by Walzer and Hendel (2008).

The viscosity function is fundamental for the evolution of the system. Some features of this function are as follows.

(a) A chemically homogeneous layer of the mantle cannot have a constant viscosity, because of the pressure dependence of the activation enthalpy. Therefore, the viscosity usually increases with pressure. Compensation or even over-compensation for the temperature dependence is only possible near the CMB because of the extremely high temperature gradient in the D" layer.
(b) Viscosity discontinuities only occur in chemically homogeneous parts of the mantle at phase boundaries, because P and T do not show stepwise changes.
(c) At depths of 410, 520, and 660 km, the olivine lattice changes to a denser packing of atoms. Therefore, it would be incorrect to assume that there are only stepwise changes in seismic velocities, v_s and v_p, and the density, ρ, but not for the activation energy and volume. Given that the activation enthalpy is in the exponent of the viscosity function, we expect appreciable viscosity stepwise changes to occur.

Walzer and Hendel (2013) introduced a new master function for viscosity, called function η_4, which is based on the above constraints. For the numerical computations, we used the following:

$$\begin{aligned}\eta=\eta(r,\theta,\varphi,t) &= 10^{r_n}\cdot\frac{exp(c\ \overline{T_m/T_{av}})}{exp(c\ \overline{T_m/T_{st}})}\cdot\eta_4\left(r\right)\cdot\\ &\cdot\quad exp\left[c_t\cdot T_m\left(\frac{1}{T}-\frac{1}{T_{av}}\right)\right]\end{aligned} \tag{7}$$

where r is the radius, θ is the co-latitude, φ is longitude, t is time, r_n is the viscosity level parameter, c_t and $c=7$ are parameters, T_m is the melting temperature, T_{av} is the laterally averaged temperature, T_{st} is the starting temperature, and η_4 is the radial viscosity profile.

The viscosity function, η_4, resembles the viscosity profile of Mitrovica and Forte (2004), although its derivation is different. The radial dependence of viscosity, $\eta_4(r)$, is based on solid-state physics considerations. We used the mean of the relative viscosity curve between the lithosphere–asthenosphere boundary (LAB) and a depth, h, of 1250 km. The absolute value of this mean was defined as 10^{21}Pa·s (i.e., the observed Haskell value). Furthermore, the Grüneisen parameter, γ, is important for solid-state geophysics. In the present paper, γ explicitly appears in Eq. (5). However, it is more important that the slope of the fusion curve, as a function of pressure, depends strongly on the Grüneisen parameter (Gilvarry, 1956). See also Eq. (B1) in Appendix B. Therefore, the melting temperature, T_m, depends strongly on the Grüneisen parameter, γ. Inserting T_m into Eqs. (7), (6), (5), and (3)), in that order, demonstrates the significance of γ for mantle–crust evolution. Prior to 2013, we utilized the Vashchenko–Zubarev gamma, γ_{VZ}. However, because the shear modes provide an essential contribution to γ, we have replaced γ_{VZ} with the acoustic gamma, γ_a, as follows:

$$\begin{aligned}\gamma_a &= \frac{1}{6}\frac{K_T}{K_S+(4/3)\mu}\left[\left(\frac{\partial K_S}{\partial P}\right)_T+\frac{4}{3}\left(\frac{\partial\mu}{\partial P}\right)_T\right]\\ &+\frac{1}{3}\frac{K_T}{\mu}\left(\frac{\partial\mu}{\partial P}\right)_T-\frac{1}{6}\end{aligned} \tag{8}$$

The quantity K_S is the adiabatic bulk modulus, K_T is the isothermal bulk modulus, and μ is the shear modulus. For the depth interval between 771 and 2741 km, we used the Preliminary reference Earth model PREM (Dziewonski and Anderson, 1981) and Eq. (8) to determine γ_a. PREM was derived from geophysical observatory measurements. For h<771 km and in the thin D" layer immediately above the CMB, the observed dK/dP and $d\mu/dP$ of PREM lead to physically implausible depth variations of γ. Therefore, we used the gamma estimates of Stacey and Davis (2009) for these depth ranges. The combined Grüneisen parameter is called the extended acoustic gamma, γ_{ax}. The basis of the approach outlined here is to utilize measured quantities to avoid assumptions, as far as possible. For example, we applied Eq. (8) to estimate the Grüneisen parameter. In this case, it is not required to assume the mantle mineralogy because the input parameters are well known from seismology. For the lower mantle, our quantity γ_{ax} lies between the gamma of Stacey and Davis (2009) and the Debye gamma. The differences between the three γ curves are small, as shown in Fig. B2 of Appendix B. However, in the case of the heat generation rate per unit volume, Q, geochemical considerations are necessary. Here we present only a brief outline of our approach. The formation of basaltic oceanic crust occurs by single-stage melting of the depleted mantle (DM) near a mid-ocean ridge (MOR). According to Hofmann (2003), 30% to 80% of Earth's mantle is depleted mantle (DM) in terms of incompatible elements (e.g., U, Th, K, and rare earth elements), although Bennett (2003) suggested the proportion is 30% to 60%. The low-viscosity asthenosphere consists preferentially of DM as verified by observations at MORs. However, the production of continental crust (CC) is much more complex. Furthermore, the chemical composition of the lower continental crust (LCC) is poorly constrained. It is assumed to be andesitic or andesitic-basaltic in composition (i.e., about 56.5 wt.% SiO_2). A minimum of two stages of chemical differentiation is necessary to produce the granodiorite-dominated upper continental crust (UCC).

We did not include specific CC differentiation mechanisms in our

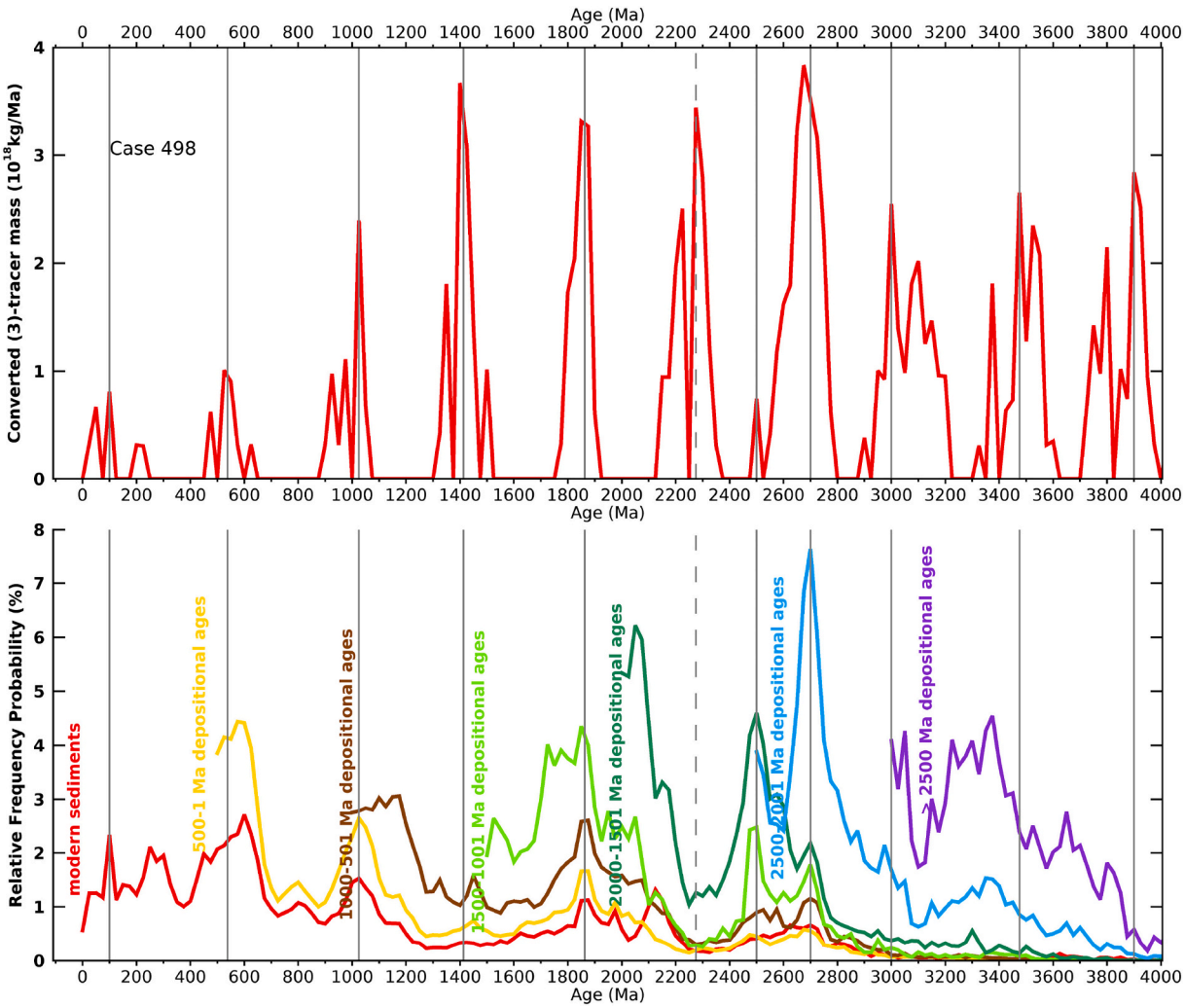

Fig. 1. Comparison of our mantle–crust evolution model based on theoretical physics (upper panel) with the observed global detrital zircon age distributions (lower panel) from Puetz and Condie (2019). The red line in the upper panel shows episodes of juvenile magmatism, which result in a new contribution to the continental crust. The lower panel is for zircon ages where the probabilities have 25 Ma bins. The colored curves are as follows: lower red = modern sediments; yellow = 500–1 Ma depositional ages; brown = 1000–501 Ma depositional ages; light green = 1500–1001 Ma depositional ages; dark green = 2000–1501 Ma depositional ages; blue = 2500–2001 Ma depositional ages; purple = depositional ages older than 2500 Ma. (For interpretation of the references to color in this figure legend, the reader is referred to the web version of this article.)

global convection model, but instead undertook this in a simplified way. We designed a dynamic 3D spherical-shell convection model of Earth's mantle and incorporated the solidus, T_{sol}, for peridotite (Litasov, 2011), which is not only a function of pressure, P, but also of the water concentration. Variable water contents are rarely considered in truly dynamic models. Compare Fig. B1 of Appendix B. Large-scale partial melting occurs only under the following condition:

$$T > f_3 \cdot T_m \tag{9}$$

or when the total water abundance exceeds the water solubility (Litasov, 2011; Mierdel, 2006; Mierdel et al., 2007). The quantity f_3 is a parameter that is somewhat smaller than or equal to one, and that we vary in different Terra runs. Given that large amounts of water escape during each chemical differentiation event, the solidus will be increased for some time after the differentiation event. We used a concept for chemical mantle reservoirs that is considerably different than in previous studies (e.g., Hofmann, 2003). We did not assume abrupt boundaries between the reservoirs, but defined the time-dependent chemical composition of a specific mantle location from the mixing ratio of the conventional reservoirs using their concentrations of incompatible elements, taken from McCulloch and Bennett (1994). We considered three chemical mantle reservoirs (CC, DM, and PM) with different abundances (Walzer and Hendel, 2013, 2017) of the heat-producing elements U, Th, and K. The segregation processes act to rapidly change the distribution of these elements, and the resulting distribution is slowly modified by solid-state mantle convection. As such, solid-state creep is slowly replenishing the DM area with radioactive elements. Given that the heat generation rate per unit volume, Q, depends on the temporally and spatially variable abundances of U, Th, and K, there is a feedback between the convection and thermal evolution of the mantle. Our model is based on a numerical solution of the balance equations of energy, momentum, moment of momentum, and mass in a spherical shell, which represents Earth's mantle. Furthermore, we use equations that conserve the four sums of the number of atoms of the pairs ^{238}U–^{206}Pb, ^{235}U–^{207}Pb, ^{232}Th–^{208}Pb, and ^{40}K–^{40}Ar.

4. Results

Puetz and Condie (2019) presented time-series analyses of seven global isotopic databases, for zircon Lu–Hf isotope data, whole-rock Sm–Nd isotope data, U–Pb detrital zircon ages, U–Pb igneous zircon ages, U–Pb non-zircon ages, whole-rock Re–Os isotope data, and LIP

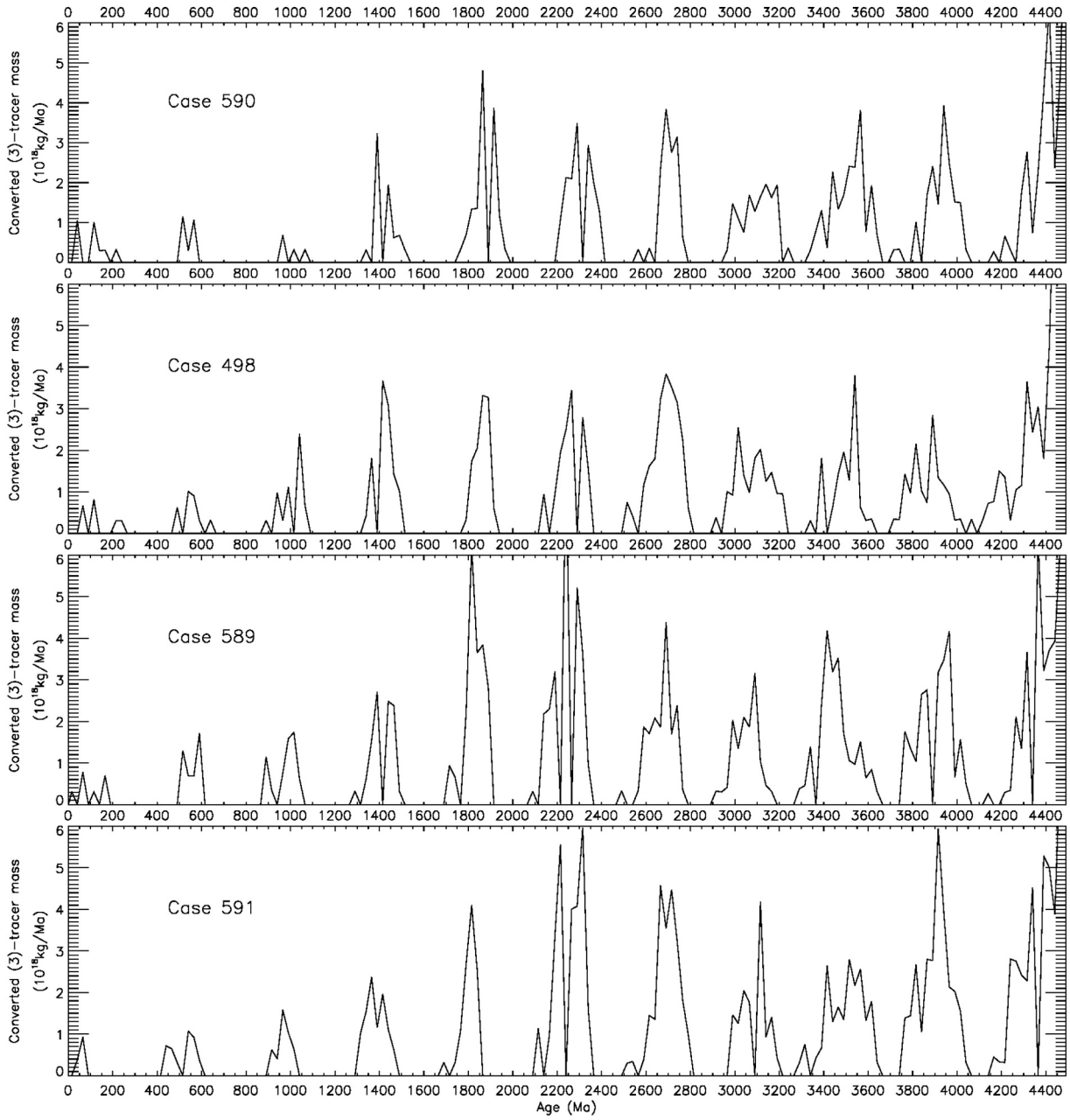

Fig. 2. Example of the effects of varying the input parameters on the chronological sequence of episodes of juvenile magmatism that contributed to continental growth. We varied the melting criterion parameter, f_3, from 0.997 (top panel) to 0.991 (bottom panel) in steps of 0.002. The visco-plastic yield stress, $\sigma_y = 120$ MPa, viscosity level parameter, $r_n = 0.5$, and mantle thermal conductivity, $k = 5.0$ W/(m·K), were kept constant.

ages. Thus, these databases expand those of Condie et al. (2015). Parman (2015) also examined a large database of detrital zircon U–Pb ages (n > 200,000) and found peaks at similar ages. In our dynamic computer model, we varied the input parameters in (Ra, σ_y, k, f_3) space, where Ra is the Rayleigh number of the mantle, σ_y is the viscoplastic yield stress of the lithosphere, k is the thermal conductivity of the mantle, and f_3 is the inequality parameter (9). The laterally averaged surface heat flow density, *qob*, temperature profile, and the number, size, form, distribution, and surface velocities of the continents are the results. No constraints were prescribed. It is remarkable that *all* the computed output parameters converge to the observed parameters, if we approach a certain point in (Ra, σ_y, k, f_3) space. The corresponding computer run is case 498. The newly produced continental mass exhibits *episodic* temporal distribution in all runs. Fig. 1 compares case 498 with the global detrital zircon age distribution of Puetz and Condie (2019). It is obvious that in addition to the calculated thermal and chemical evolution of the mantle, the different preservation potential of crustal rocks is important in controlling the temporal distribution of the observed zircon ages. Therefore, it is unsurprising that for ages older than 2900 Ma our calculated continental increments are greater than those observed from the zircon ages. However, *all* our runs exhibit similar patterns, with episodes of strong juvenile continental crustal growth interrupted by periods of quiescence. This applies to all physically meaningful combinations of input parameters. Therefore, we propose *that the series of peaks and troughs in the global detrital zircon age distribution of Puetz and Condie (2019) are largely produced by chemical differentiation in temporarily (partially) molten regions of the upper mantle* (Fig. 1). *As such, the growth of continental crust was episodic rather than steady state*, in contrast to the conclusions of Cawood et al. (2013). In some time periods, we obtain a good correspondence between the observed and computed peak ages.

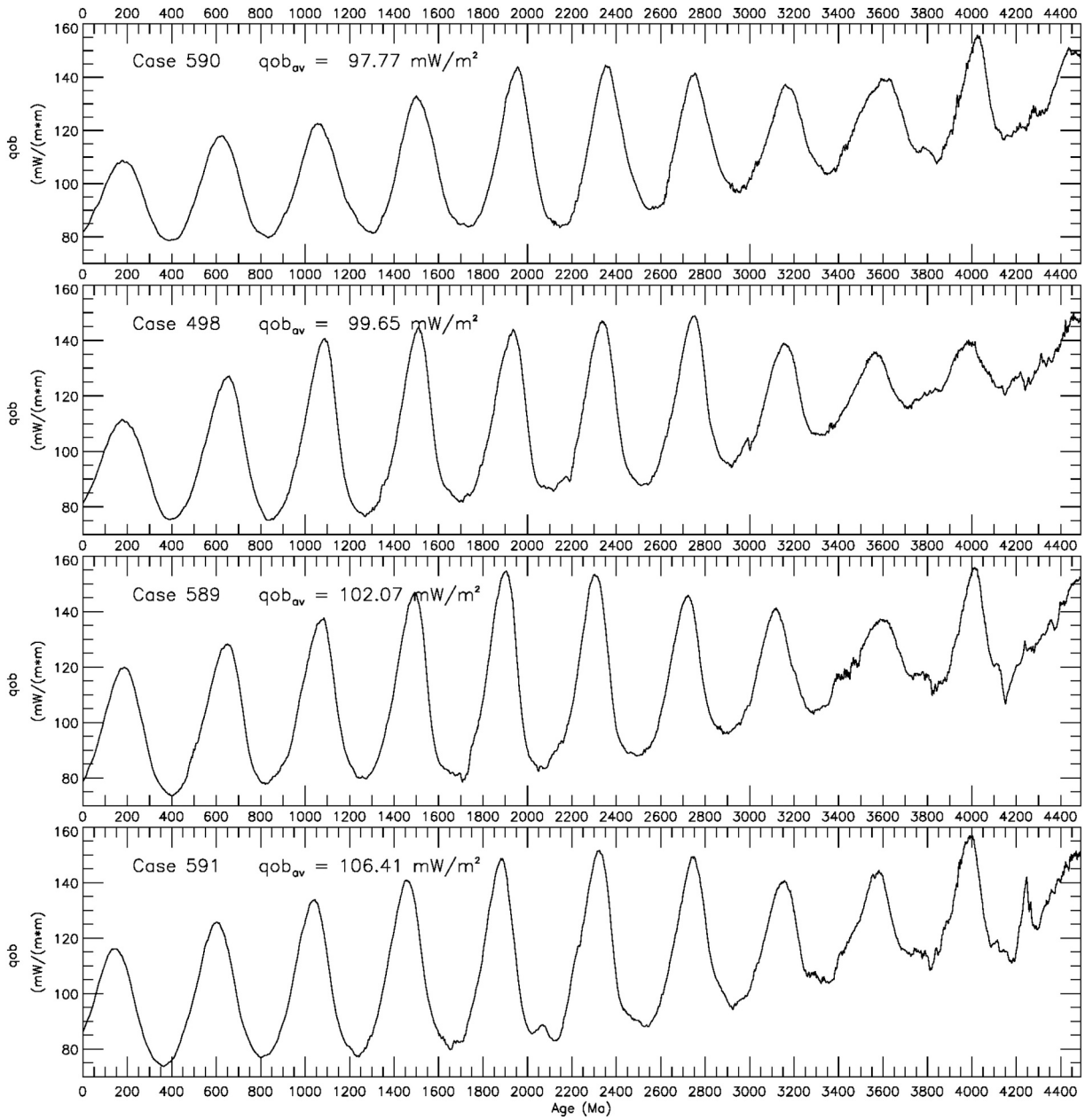

Fig. 3. Evolution of the laterally averaged heat flow density, *qob*, at Earth's surface. The curves were computed with varying f_3 from 0.997 (top panel) to 0.991 (bottom panel) in steps of 0.002. The quantities $\sigma_y = 120$ MPa, $r_n = 0.5$, and $k = 5.0$ W/(m K) were kept constant. The temporal average of *qob* for the last 200 Ma is referred to as qob_{av}.

This is notable because our input parameters only apply within assigned uncertainty boundaries.

The fact that only from an age of 2900 Ma onwards the observed and the calculated growth curve of the continents essentially agree, could possibly also have to do with the earlier considerably stronger recycling of continental material back into the mantle and a change in the chemical composition of the upper continental crust. Nebel et al. (2018) show that there was a profound change in crustal chemistry thereafter. Around 2760 Ma, transitional TTGs (tonalites, trondhjemites, and tonalites) are observed, followed soon after by sanukitoids. Soon thereafter, underplating is observed to a greater extent. Cawood et al. (2018) show that the transition from TTGs on the one hand to sanukitoids, hybrid granitoids and Bi and 2 mica granitoids on the other is not exactly simultaneous. The transition in the Pilbara region was earlier than in most other areas.

It is not important to understand Eqs. (1)–(9) in simple terms and why the solutions yield episodic events. Eqs. (1)–(6) represent the basic equations of classical fluid dynamics for infinite Prandtl numbers, Eqs. (7) and (8) are advantageous in that we can extrapolate the Haskell value of viscosity using observed seismic data downward to the CMB. All geophysical parameters necessary for the calculations are provided in Appendix B. These are based on robust measurements, which of course have uncertainties. To be precise: it is neither necessary nor possible to explain the whole system exactly in words. One must understand the principles of physics. And even then it is not possible to explain the exact location of the spacings of the events in words.

One advantage of our methodology is that it is not possible to adjust the numerical results to fit the observations (i.e., in this case the distribution of zircon ages). Moreover, the correct present-day continental mass and laterally averaged surface heat flow density were both obtained in the same computer run. In addition, the laterally averaged present-day temperature as a function of depth corresponds

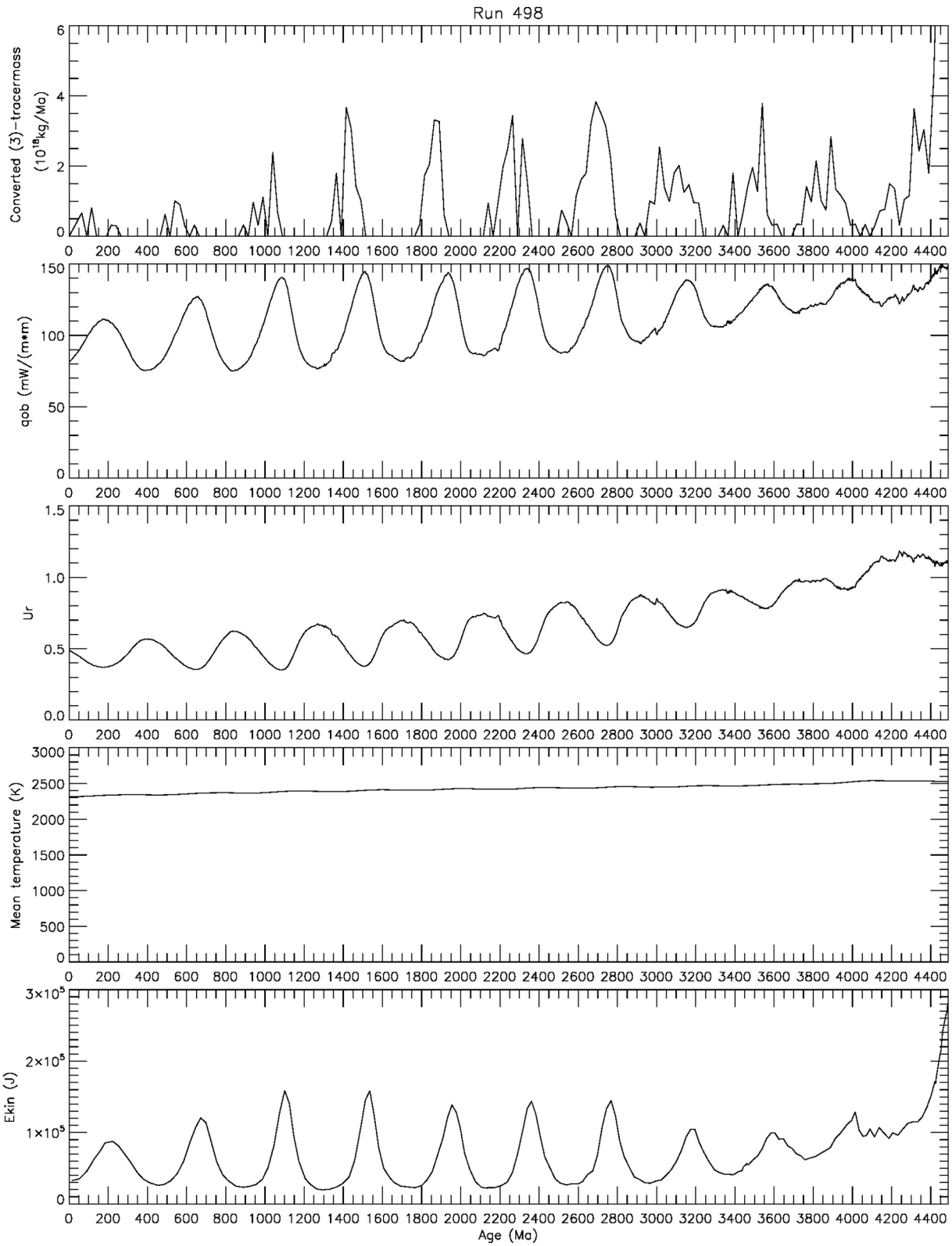

Fig. 4. Evolution curves for case 498. For this run, the viscosity level parameter was $r_n = 0.5$. This corresponds to a Rayleigh number, *Ra*, of approximately 10^8. The visco-plastic yield stress is $\sigma_y = 120$ MPa, the thermal conductivity of the mantle is $k = 5.0$ W/(m K), and $f_3 = 0.995$. The first panel shows the juvenile contributions to the continental crust; the second panel shows the laterally averaged surface heat flow density, *qob*; the third panel shows the Urey number, *Ur*; the fourth panel highlight the slow decrease of T_{mean} (i.e., the volumetrically averaged mantle temperature); the fifth panel shows the kinetic energy, E_{kin}, of mantle convection.

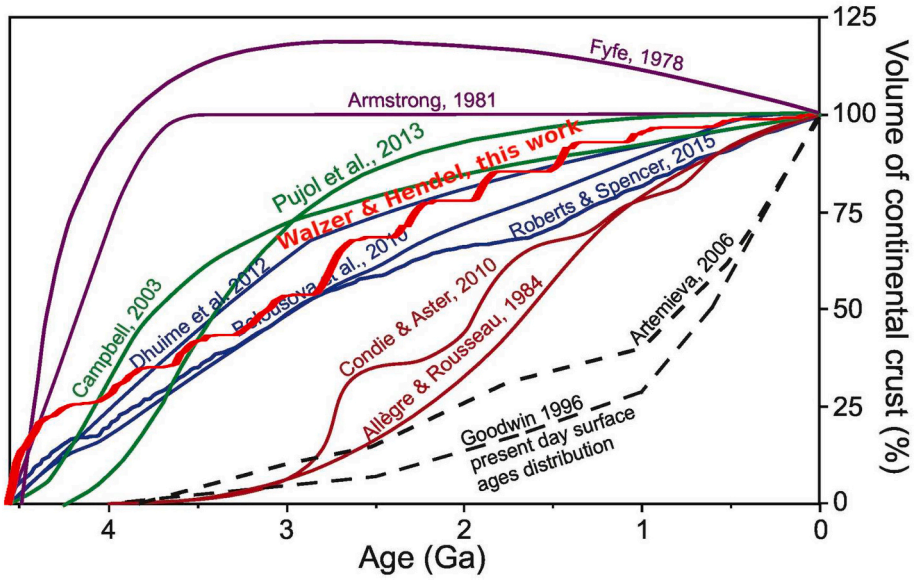

Fig. 5. Comparison of our computed curve for continental crustal growth (red) and various crustal growth model curves compiled by Cawood and Hawkesworth (2019). Violet curves = Fyfe (1978) and Armstrong and Harmon (1981); green curves = Campbell (2003) and Pujol et al. (2013), blue curves = Belousova et al. (2010), Dhuime et al. (2012), and Roberts and Spencer (2015); brown curves = Allegre and Rousseau (1984) and Condie and Aster (2010); black dashed curves = Goodwin (1996) and Artemieva (2006). (For interpretation of the references to color in this figure legend, the reader is referred to the web version of this article.)

approximately to other estimates (Katsura, 2022). Given the tight nesting of the system of equations, it is encouraging to note the similarity of our calculated results with the global detrital zircon age distribution of Puetz and Condie (2019) (Fig. 1).

We also varied the input parameters to our model, and some results are presented in Figs. 2 and 3. In a physical system, all processes are intrinsically linked. Therefore, we make a point of showing that the run which produced the good accord with the observed global isotopic data (Fig. 1), generates also other reasonable results. In Fig. 4, we compare the evolution of the mass of newly generated continental crust; laterally averaged heat flow density, *qob*, at Earth's surface; Urey number, *Ur*; volumetrically averaged temperature, T_{mean}, of the mantle and crust; and kinetic energy, E_{kin}, of solid-state convection in the mantle. As a result, there are magmatically quiescent intervals between the active periods (Fig. 4). Furthermore, *qob*, *Ur*, and E_{kin} show distinct sinusoidal curves over time, superimposed on a slowly decreasing trend (Fig. 4). However, the volumetrically averaged mantle temperature, T_{mean}, *does not change rapidly and decreases monotonously* (cf. Fig. 4, fourth panel). This result is consistent with the findings of Gurnis and Davies (1986). Therefore, we can dismiss catastrophic mechanisms that *simultaneously* involve the entire mantle. The third panel of Fig. 4 exhibits our present-day Urey number (i.e., the mantle heat production divided by the heat loss at the surface) is somewhat lower than 0.5. Conventional Urey ratio estimates are 0.21–0.49. However, Lenardic et al. (2011) showed that convection simulations *with* continents lead to Urey ratio estimates of 0.33–0.76. Lay et al. (2008) estimated the total heat flow at Earth's surface to be 43–49 TW. This corresponds to a present-day *qob* of 84.3–96.1 mW/m^2. Davies and Davies (2010) preferred an estimate of 47 ± 2 TW.

Various approaches have been used to estimate the temporal evolution of the volume of continental crust (Fig. 5). The models of Fyfe (1978) and Armstrong and Harmon (1981) assume that the continental crust formed rapidly during the Hadean, and that its evolution was controlled solely by recycling. Fyfe (1978) concluded from his somewhat simple model that the continents originated in the Hadean and that their total mass decreased slightly during Earth history. In contrast, the

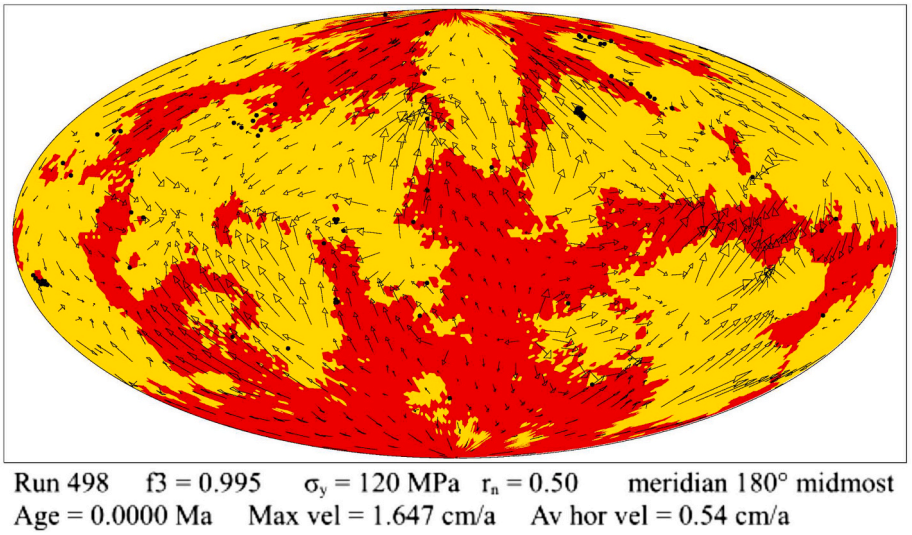

Fig. 6. Present-day distribution of the continents (red), oceanic lithosphere (yellow), and oceanic plateaus (black dots) for run 498. The quantities $r_n = 0.5$, $\sigma_y = 120$ MPa, $k = 5.0$ W/(m·K), and $f_3 = 0.995$ were kept constant. The arrows show the present-day creep velocities at the surface. (For interpretation of the references to color in this figure legend, the reader is referred to the web version of this article.)

Goodwin (1996) and Artemieva (2006) models were based on the present-day distribution of ages and thickness of continental crust, and did not consider the paucity of the early record. Similarly, the Condie and Aster (2010) model was inferred from *presently preserved* rocks with different Nd and Hf isotopic ages. The Allegre and Rousseau (1984) model was derived from the Nd isotope ratios of Australian shales. Belousova et al. (2010) suggested that Hf model ages could be used as a proxy for continental crustal growth. However, Arndt and Davaille (2013) disputed this, because an analysis of associated epsilon Hf(t) values indicated that nearly all zircons are contaminated to various degrees by crustal reworking, which combines two or more age components of the continental crust without resetting the zircon ages in the host rocks. To alleviate this problem, Korenaga (2018) proposed an unmixing model to constrain the juvenile component of continental crust, and concluded that crustal production is episodic. In a slightly different approach, Dhuime et al. (2012) and Roberts and Spencer (2015) used the radiogenic U–Pb and Lu–Hf isotope systems in combination with $\delta^{18}O$ data. While each approach has its own limitations, collectively the methods clarify the possible mechanisms for the evolution of continental crust. We propose that the blue curves (Belousova et al., 2010; Dhuime et al., 2012; Roberts and Spencer, 2015) in Fig. 5 are a good approximation. However, *our* model is deduced quite differently. It is based on theoretical physics. It is notable that our red evolution curve plots between the blue curves for most of the period of mantle evolution. The episodic nature of the red curve is evidently realistic because of Fig. 1. We also suggest that the high initial rate of crustal generation during the Hadean is realistic. Fig. 6 shows a representative present-day distribution of continental and oceanic crust, and oceanic plateaus. At present, the *computed* continents cover 42.2% of Earth's surface. According to Head (1990), the *observed* continental crustal area of Earth is 41% of its surface. If we include the continental slope down to 2000 m depth as being continental in nature, then 40.7% of Earth's surface is covered by continents.

We now want to extend the comparison of our episodes of continental crust formation, *calculated* on a theoretical-physical basis, shown in Fig. 1, with further *observational* data. Puetz and Condie (2022) enlarged the detrital zircon databases (DB) of Voice et al. (2011) and Roberts and Spencer (2015) and combined them with the DB of Puetz and Condie (2019) and Puetz and Condie (2021) to create a DB with nearly one million records. Fig. 7 shows a comparison of our theoretical curve with the new combined DB. At this point, it is perhaps appropriate to make a few basic comments. This is because the conclusions drawn from them are not always taken into account in geology. It is now generally accepted that thermal convection in the Earth's mantle is the main cause of lithospheric plate motions, orogenesis, and even Archean tectonic phenomena that do not conform to the rules of plate tectonics. The convection, in turn, is a consequence of the thermodynamics of the mantle. The basis of all thermodynamics are the four main laws.

The zeroth law is: The system A is in thermal equilibrium with the system B. The system B is in thermal equilibrium with the system C. If these two statements are fulfilled, it follows that the two systems A and C must also be in thermal equilibrium with each other.

The first law reads: The change in internal energy of a closed system is equal to the sum of the change in heat and the change in mechanical work. This is the theorem of conservation of energy.

The second law is: There is no change of state whose only result is the transfer of heat from a body of lower temperature to a body of higher temperature. Or: It is not possible to construct a cyclically operating machine that produces no effect other than the transfer of heat from a colder to a warmer body. This is the entropy theorem. In a closed system, entropy can only increase or remain the same. The latter happens *only* if there is no friction or other conversion of kinetic and potential energy into heat. In geology, entropy always increases, that is, without any exception.

The third law of thermodynamics states that absolute zero of temperature cannot be obtained by any process with a finite number of steps. Absolute zero can be approached at will, but never obtained.

Let us now apply these principles to the evolution of the Earth. After the Late Heavy Bombardment, the condensed Earth can be considered essentially as a closed system. Of course, this does not apply to the higher layers of the atmosphere, but their mass fraction is very small anyway. The law of conservation of energy applies to a closed system. We have expressed this in this paper by Eq. (4). The entropy theorem is of equally fundamental importance: In an adiabatically closed system, entropy cannot decrease, it usually increases. Only in reversible processes it remains constant. *Exactly periodic processes belong to the reversible processes* and are only possible if no conversion of kinetic or potential energy into heat takes place. This is approximately fulfilled, for example, in the motion of the planets around the Sun. If, for example, medium- and short-period variations of the natural climate and consequently of the temporal succession of sediments are controlled by celestial mechanics of the planets, then a periodic succession will be observed. Hinnov (2018) and Laskar (2020) show that major contributions to the geological time scale derive e.g. from a principal metronome generated by interactions of the orbital perihelia of Venus and Jupiter, $g_2 - g_5$, with a period of 405 ka. This effect is found in the cyclostratigraphy dominated by precession and orbital eccentricity forcing. Another metronome comes from the orbital inclinations of Earth and Saturn, $s_3 - s_6$, with a period of 173 ka, which is also found in the succession of sediments. Similar medium- and short-period periodicity is also found in the banded iron formations and cap carbonates after the snowball Earth ages (Mitchell et al., 2021). However, one should not expect to find this cyclicity in processes controlled by the thermal evolution of the Earth's mantle, where entropy is strongly increasing. The effective viscosity (cf. Eq. (7)) of solid-state creep in the Earth's mantle causes a dissipation of convection energy. The energy sources of mantle convection, expressed in the present paper by the quantity Q, are also decreasing due to the laws of radioactive decay. *Therefore, it is not at all curious if magmatic activity decreases in recent times and, moreover, is distributed episodically rather than periodically.* If one examines any time series with Fourier analysis, one will always get periodic proportions. But this is no proof for a really periodic process, which can exist for fundamental physical reasons only for reversible processes. If one has found out periods by a merely mathematical procedure, for example by a Fourier analysis, then this is a good orientation aid, but no proof for a periodic process in a physical sense. The *episodic* nature of continental crust production is evidently realistic because of Figs. 1 and 7.

Our key findings are as follows:

a) We show that it is possible to derive the thermal evolution of the mantle and the formation of the continents from a unified system of equations. This numerical system is based on the complete set of balance equations of physics.
b) Continental growth was an episodic rather than steady state process.
c) The computed timings of continental growth are similar to the observed global detrital zircon ages given by Puetz and Condie (2019, 2022).
d) The above three key findings also occur in computer runs that do not contain the following additional condition. We now introduce an additional realistic dependence of mantle solidus on water abundance and pressure (compare Fig. B1 of Appendix B). This additional dependence is based on measurements. Each calculated chemical differentiation event abruptly decreases the water concentration of the relevant mantle region. This is, of course, because partial or total melting in magma chambers is associated with degassing, which can be considered quasi-instantaneous on this time scale.

Fig. B1 of Appendix B shows that this rapid decrease in water abundance causes a sharp increase in the melting temperature, T_m, in the specified area. Eq. (7) in turn indicates that the effective viscosity then also increases rapidly in the given area. Therefore, it then takes some time for the slow solid-state creeping of the mantle convection and, in

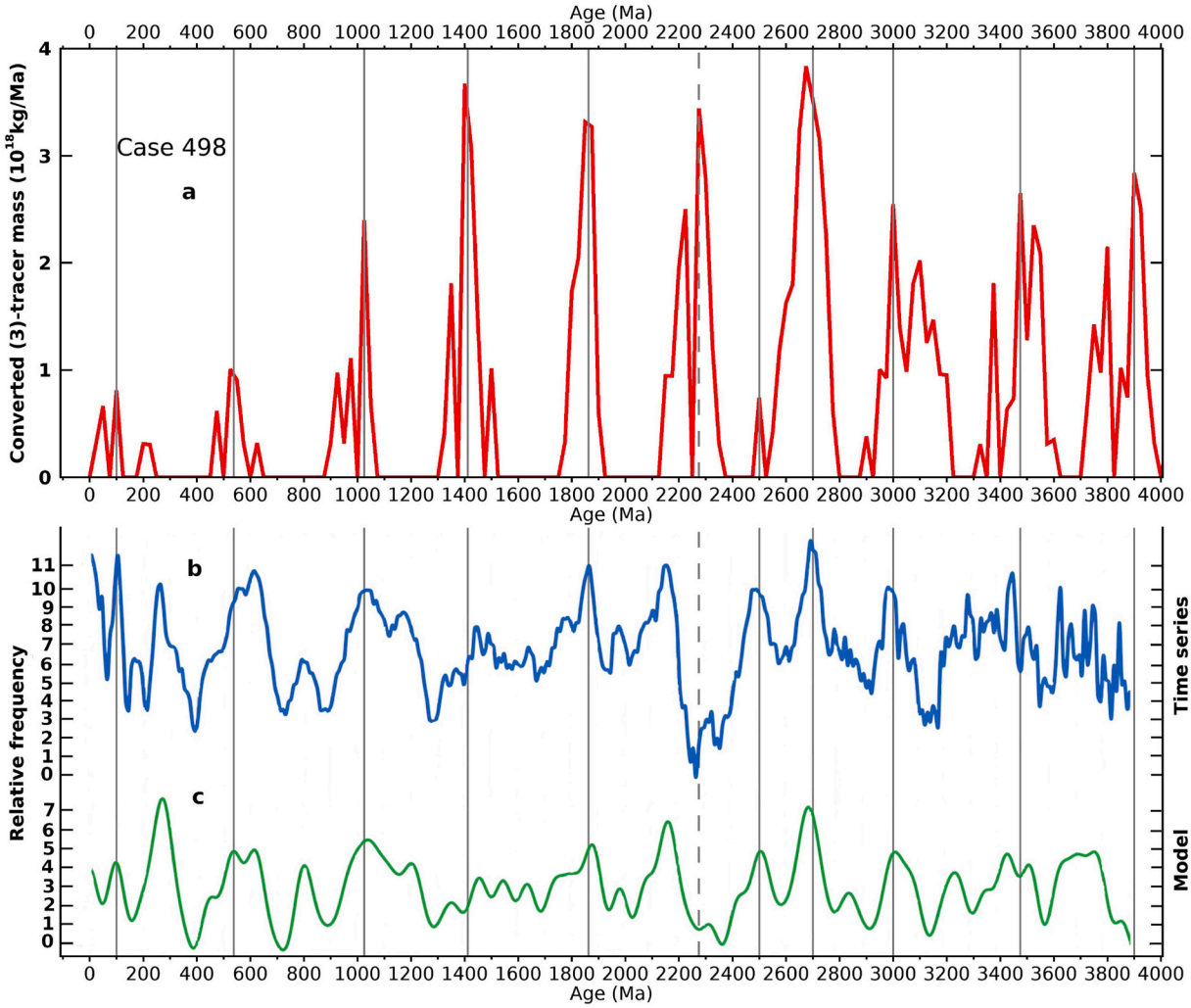

Fig. 7. Comparison of our computed mantle-crust evolution model (panel a) with the observed global detrital zircon U-Pb age distribution and the low-frequency Model 2 of Puetz and Condie (2022). Time series for the 3900-0 Ma interval, binned at 10-Ma intervals. Panel b: Bandpass-filtered U-Pb age distribution from Combined-DB. Panel c: Low frequency model. Correlation coefficient = 0.788. (For interpretation of the references to color in this figure legend, the reader is referred to the web version of this article.)

the special case, subduction to bring more water-rich material into the particular space region. Only after solid-state convection has slowly introduced more water-rich material into the previously melted mantle region can a new chemical differentiation event occur. This is the reason that for runs with the mentioned additional assumption time intervals of magmatic quiescence occur. The most important result, however, is that *the temporal distribution of juvenile crustal additions to the continents, as determined using our model, is similar to the global detrital zircon ages compiled by Puetz and Condie (2019, 2022)* (cf. Figs. 1 and 7).

Declaration of Competing Interest

The authors declare that they have no known competing financial interests or personal relationships that could have appeared to influence the research reported in this paper.

Acknowledgements

We gratefully acknowledge the longstanding, confidential collaboration with John Baumgardner. We thank Dave Stegman for providing his particle code. We also thank SCC Karlsruhe and HLRS Stuttgart for the use of their supercomputing facilities. This research was partly supported by the Deutsche Forschungsgemeinschaft (Grants WA1035/5-3 and KL495/16-1). We thank the reviewers for their fair comments and useful suggestions.

Appendix A. Supplementary data

Supplementary data to this article can be found online at doi:10.1016/j.earscirev.2022.104130.

References

Albarède, F., 1998. The growth of continental crust. Tectonophysics 296 (1–2), 1–14.
Allegre, C.J., Rousseau, D., 1984. The growth of the continent through geological time studied by Nd isotope analysis of shales. Earth Planet. Sci. Lett. 67, 19–34.
Armstrong, R., Harmon, R., 1981. Radiogenic isotopes: The case of crustal recycling on a near-steady-state no-continental-growth Earth [and discussion]. Philosophical Transactions of the Royal Society of London A: Mathematical. Phys. Eng. Sci. 301, 443–472.
Arndt, N., Davaille, A., 2013. Episodic Earth evolution. Tectonophysics 609, 661–674.
Artemieva, I.M., 2006. Global 11 thermal model TC1 for the continental lithosphere: Implications for lithosphere secular evolution. Tectonophysics 416 (1–4), 245–277.
Asplund, M., Grevesse, N., Sauval, A.J., Scott, P., 2009. The chemical composition of the Sun. Annu. Rev. Astron. Astrophys. 47, 481–522. https://doi.org/10.1146/annurev.astro.46.060407.145222.
Baumgardner, J.R., 1983. A Three-Dimensional Finite Element Model for Mantle Convection. Ph. D. thesis. University of California, Los Angeles.

Belousova, E.A., Kostitsyn, Y.A., Griffin, W.L., Begg, G.C., O'Reilly, S.Y., Pearson, N.J., 2010. The growth of the continental crust: Constraints from zircon HF-isotope data. Lithos 119 (3–4), 457–466.
Bennett, V.C., 2003. Compositional evolution of the mantle, in: Carlson, R.W. Treatise on Geochemistry, Vol. 2: The Mantle and the Core. Elsevier, Amsterdam, pp. 493–519.
Bunge, H.P., Baumgardner, J.R., 1995. Mantle convection modelling on parallel virtual machines. Comput. Phys. 9, 207–215.
Campbell, I.H., 2003. Constraints on continental growth models from Nb/U ratios in the 3.5 Ga Barberton and other Archaean basalt-komatiite suites. Am. J. Sci. 303 (4), 319–351 doi: 10.2475/ajs.303.4.319.
Cawood, P.A., Hawkesworth, C.J., 2019. Continental crustal volume, thickness and area, and their geodynamic implications. Gondwana Res. 66, 116–125. https://doi.org/10.1016/j.gr.2018.11.001.
Cawood, P.A., Hawkesworth, C.J., Dhuime, B., 2013. The continental record and the generation of continental crust. Geol. Soc. Am. Bull. 125 (1/2), 14–32. https://doi.org/10.1130/B30722.1.
Cawood, P.A., Hawkesworth, C.J., Pisarevsky, S.A., Dhuime, B., Capitanio, F.A., Nebel, O., 2018. Geological archive of the onset of plate tectonics. Philosophical Transactions of the Royal Society A: Mathematical. Phys. Eng. Sci. A 376 (20170405), 1–30. https://doi.org/10.1098/rsta.2017.0405.
Condie, K.C., Arndt, N., Davaille, A., Puetz, S.J., 2017. Zircon age peaks: Production or preservation of continental crust? Geosphere 13 (2), 227–234.
Condie, K.C., Aster, R.C., 2010. Episodic zircon age spectra of orogenic granitoids: the supercontinent connection and continental growth. Precambrian Res. 180 (3-4), 227–236. https://doi.org/10.1016/j.precamres.2010.03.008.
Condie, K.C., Belousova, E., Griffin, W., Sircombe, K.N., 2009. Granitoid events in space and time: constraints from igneous and detrital zircon age spectra. Gondwana Res. 15, 228–242.
Condie, K.C., Davaille, A., Aster, R.C., Arndt, N., 2015. Upstairs-downstairs: supercontinents and large igneous provinces, are they related? Int. Geol. Rev. 57, 1341–1348. https://doi.org/10.1080/00206814.2014.963170.
Condie, K.C., Pisarevsky, S.A., Puetz, S.J., 2021. LIPs, orogens and supercontinents: The ongoing saga. Gondwana Res. 96, 105–121.
Davies, J.H., Davies, D.R., 2010. Earth's surface heat flux. Solid Earth 1, 5–24.
Dhuime, B., Hawkesworth, C.J., Cawood, P.A., Storey, C.D., 2012. A change in the geodynamics of continental growth 3 billion years ago. Science 335 (6074), 1334–1336.
Dziewonski, A.M., Anderson, D.L., 1981. Preliminary reference Earth model. Phys. Earth Planet. Inter. 25, 297–356.
Fyfe, W.S., 1978. The evolution of the Earth's crust: Modern plate tectonics to ancient hotspot tectonics? Chemical Geology 23 (1–4), 89–114.
Gilvarry, J.J., 1956. Equation of the fusion curve. Phys. Rev. 102 (2), 325–331. https://doi.org/10.1103/PhysRev.102.325.
Goodwin, A.M., 1996. Principles of Precambrian Geology. Academic Press, London, p. 327.
Gurnis, M., Davies, G.F., 1986. Apparent episodic crustal growth arising from a smoothly evolving mantle. Geology 14, 396–399.
Hawkesworth, C., Cawood, P., Kemp, T., Storey, C., Dhuime, B., 2009. A matter of preservation. Science 323, 49–50.
Hawkesworth, C., Cawood, P.A., Dhuime, B., 2019. Rates of generation and growth of the continental crust. Geosci. Front. 10 (1), 165–173.
Head, J., 1990. Venus hypsometric curve: an assessment of its components and comparison to Earth.. In: Lunar and Planetary Science Conference XXI, p. 479.
Heisenberg, W., 1926a. Mehrkrperproblem und Resonanz in der Quantenmechanik. Zeitschrift fr Phys. 38, 411–426. https://doi.org/10.1007/BF01397160.
Heisenberg, W., 1926b. ber die Spektra von Atomsystemen mit zwei Elektronen. Zeitschrift fr Phys. 39, 499–518. https://doi.org/10.1007/BF01322090.
Hinnov, L.A., 2018. Cyclostratigraphy and Astrochronology in 2018. In: Stratigraphy & Timescales. volume 3. Elsevier, pp. 1–80.
Hofmann, A.W., 2003. Sampling mantle heterogeneity through oceanic basalts: Isotopes and trace elements, in: Carlson R.W. Treatise on Geochemistry, Vol. 2: The Mantle and the Core. Elsevier, Amsterdam, pp. 61–101.
Jiang, D., Tian, Z., Lang, X., 2016. Reliability of climate models for China through the IPCC Third to Fifth Assessment Reports. Int. J. Clim. 36, 1114–1133.
Katsura, T., 2022. A revised adiabatic temperature profile for the mantle. J. Geophys. Res.: Solid Earth 127, 1–11 e2021JB023562.
Korenaga, J., 2018. Estimating the formation age distribution of continental crust by unmixing zircon ages. Earth Planet. Sci. Lett. 482, 388–395. https://doi.org/10.1016/j.epsl.2017.11.039.
Laskar, J., 2020. Astrochronology. In: Geologic Time Scale 2020. Elsevier, pp. 139–158. https://doi.org/10.1016/B978-0-12-824360-2.00004-8.
Lay, T., Hernlund, J., Buffett, B.A., 2008. Core-mantle boundary heat flow. Nat. Geosci. 1, 25–32.
Lenardic, A., Cooper, C., Moresi, L., 2011. A note on continents and the Earth's Urey ratio. Phys. Earth Planet. Inter. 188 (1–2), 127–130. https://doi.org/10.1016/j.pepi.2011.06.008.
Litasov, K.D., 2011. Physicochemical conditions for melting in the Earth's mantle containing a C-O-H fluid (from experimental data). Russian Geol. Geophys. 52, 475–492.
Lodders, K., Palme, H., Gail, H.P., 2009. Abundances of the elements in the solar system. Landoldt-Börnstein, New Series, Vol. VI / 4B, Chap. 4.4, J.E. Trümper (ed.). Springer-Verlag, Berlin, Heidelberg, New York, pp. 560–630.
McCulloch, M.T., Bennett, V.C., 1994. Progressive growth of the Earth's continental crust and depleted mantle: Geochemical constraints. Geochim. Cosmochim. Acta 58 (21), 4717–4738.
Mierdel, K., 2006. Wasserlöslichkeit in Enstatit. Ph. D. thesis. Univ. Tübingen. Tübingen, Germany.
Mierdel, K., Keppler, H., Smyth, J.R., Langenhorst, F., 2007. Water solubility in aluminous orthopyroxene and the origin of the Earth's asthenosphere. Science 315, 364–368. https://doi.org/10.1126/science.1135422.
Mitchell, R.N., Gernon, T.M., Cox, G.M., Nordsvan, A.R., Kirscher, U., Xuan, C., Liu, Y., Liu, X., He, X., 2021. Orbital forcing of ice sheets during snowball Earth. Nat. Commun. 12 (4187), 1–9. https://doi.org/10.1038/s41467-021-24439-4.
Mitrovica, J.X., Forte, A.M., 2004. A new inference of mantle viscosity based upon joint inversion of convection and glacial isostatic adjustment data. Earth Planet. Sci. Letters 225 (1), 177–189.
Morgenstern, O., Hegglin, M.I., Rozanov, E., et al., 2017. Review of the global models used within phase 1 of the Chemistry-Climate model initiative (CCMI). Geosci. Model Dev. 10, 639–671. https://doi.org/10.5194/gmd-10-639-2017.
Nebel, O., Capitanio, F., Moyen, J.F., Weinberg, R., Clos, F., Nebel-Jacobsen, Y., Cawood, P., 2018. When crust comes of age: on the chemical evolution of Archaean, felsic continental crust by crustal drip tectonics. Philosophical Transactions of the Royal Society A: Mathematical. Phys. Eng. Sci. 376, 20180103.
Parman, S.W., 2015. Time-lapse zirconography: Imaging punctuated continental evolution. Geochem. Perspect. Lett. 1, 43–52.
Puetz, S.J., Condie, K.C., 2019. Time series analysis of mantle cycles part I: Periodicities and correlations among seven global isotopic databases. Geosci. Front. 10, 1305–1326. https://doi.org/10.1016/j.gsf.2019.04.002.
Puetz, S.J., Condie, K.C., 2021. Applying Popperian falsifiability to geodynamic hypotheses: Empirical testing of the episodic crustal/zircon production hypothesis and selective preservation hypothesis. Int. Geol. Rev. 63, 1920–1950.
Puetz, S.J., Condie, K.C., 2022. A review of methods used to test periodicity of natural processes with a special focus on harmonic periodicities found in global U-Pb detrital zircon age distributions. Earth-Sci. Rev. 224 (1–35), 103885.
Pujol, M., Marty, B., Burgess, R., Turner, G., Philippot, P., 2013. Argon isotopic composition of Archaean atmosphere probes early Earth geodynamics. Nature 498, 87–90.
Reimink, J.R., Davies, J.H., Ielpi, A., 2021. Global zircon analysis records a gradual rise of continental crust throughout the Neoarchean. Earth Planet. Sci. Lett. 554, 1–11. https://doi.org/10.1016/j.epsl.2020.116654.
Roberts, N.M., Spencer, C.J., 2015. The zircon archive of continent formation through time. Geol. Soc., London, Special Publications 389, 197–225.
Rudnick, R.L., Gao, S., 2003. Composition of the continental crust, in: Rudnick R.L. Treatise on Geochemistry, Vol.3: The Crust. Editors-in-chief H. D. Holland and K. K. Turekian, 1st ed. Elsevier, Amsterdam, pp. 1–64 chapter 3.01.
Schrdinger, E., 1926a. Der stetige bergang von der Mikro- zur Makromechanik. Naturwissenschaften 28, 664–666.
Schrödinger, E., 1926. Über das Verhältnis der Heisenberg-Born-Jordanschen Quantenmechanik zu der meinen. Annalen der Phys. 79, 734–756. https://doi.org/10.1002/andp.19263840804.
Stacey, F.D., Davis, P.M., 2009. Physics of the Earth, 4th ed. Cambridge University Press, Cambridge, UK.
Strassmann, K.M., Joos, F., 2018. The Bern Simple Climate Model (BernSCM) v1.0: an extensible and fully documented open-source re-implementation of the Bern reduced-form model for global carbon cycle-climate simulations. Geosci. Model Dev. 11, 1887–1908.
Voice, P.J., Kowalewski, M., Eriksson, K.A., 2011. Quantifying the timing and rate of crustal evolution: global compilation of radiometrically dated detrital zircon grains. J. Geol. 119, 109–126.
Walzer, U., Hendel, R., 2008. Mantle convection and evolution with growing continents. J. Geophys. Res. 113, B09405. https://doi.org/10.1029/2007JB005459.
Walzer, U., Hendel, R., 2013. Real episodic growth of continental crust or artifact of preservation? A 3-D geodynamic model. J. Geophys. Res.: Solid Earth 118, 2356–2370. https://doi.org/10.1002/j.grb.50150.
Walzer, U., Hendel, R., 2017. Continental crust formation: numerical modelling of chemical evolution and geological implications. Lithos 278-281, 215–228. https://doi.org/10.1016/j.lithos.2016.12.014.
Walzer, U., Hendel, R., 2022. A review of Continental crust growth, natural climate change, and ice ages. Earth Sci. Rev. in preparation.
Walzer, U., Hendel, R., Baumgardner, J., 2004. The effects of a variation of the radial viscosity profile on mantle evolution. Tectonophysics 384, 55–90.
Wigner, E.P., 1959. Group Theory and its Application to the Quantum Mechanics of Atomic Spectra. Academic Press, New York.
Yang, W.S., 1997. Variable viscosity thermal convection at infinite Prandtl number in a thick spherical shell. Ph. D. thesis. University of Illinois, Urbana-Champaign.
Zhu, F., Emile-Geay, J., McKay, N.P., et al., 2019. Climate models can correctly simulate the continuum of global-average temperature variability. Proc. Nat. Acad. Sci. 116, 8728–8733.
Zinke, J., Emile-Geay, J., McKay, N., Kaufman, D., et al., 2017. PAGES2k Consortium, a global multiproxy database for temperature reconstructions of the Common Era. Sci. Data 4, 170088. https://doi.org/10.1038/sdata.2017.88.